



Reinforcement effect of Mg–Al–Zn ternary IMC on MB8/2024 joints with Al/Zn/Cu/Zn multi-interlayer via ultrasonic-assisted brazing

Jie LI¹, Lei SHI², Yi-nan LI¹, Tao-shuai ZHOU¹, Zi-jing YU¹,
Hong-chang ZHANG¹, Zi-long PENG¹, Shu-wen MIAO³, Jian-guo GAO³, Zhao-fang SU³

1. School of Mechanical & Automotive Engineering, Qingdao University of Technology, Qingdao 266000, China;
2. Zhejiang Asia General Soldering & Brazing Material Co., Ltd., Hangzhou 310000, China;
3. Shandong Jingdian Heavy Industry Group Co., Ltd., Jining 272100, China

Received 10 December 2021; accepted 11 April 2022

Abstract: The evolution of microstructure in the MB8/2024 dissimilar alloy joints by using Al/Zn/Cu/Zn multi-interlayers via ultrasonic-assisted brazing was investigated. The results show that the addition of aluminum foil on the MB8 side realized the transformation of Al_3Mg_2 binary intermetallic compounds (IMCs) to $AlMg_4Zn_{11}$ ternary IMCs along the interface between copper foil and MB8 magnesium alloys. This transformation reinforced the joints and then the shear strength reached a maximum at 22 s (85.26 MPa). Thermodynamic analysis shows that $\Delta G_{Mg,Al,Zn}$ of $AlMg_4Zn_{11}$ (−38.65 kJ/mol) was smaller than that of Al_3Mg_2 (−31.94 kJ/mol), which provided a basis for the IMC transformation. $Mg_{32}(Al,Zn)_{49}$ quasicrystal was found for the first time using ultrasonic-assisted brazing due to the cavitation effect.

Key words: Al/Zn/Cu/Zn multi-interlayer; ultrasonic-assisted brazing; intermetallic compound (IMC); phase transformation; mechanical performance; quasicrystal

1 Introduction

Magnesium alloys have been widely studied because of their high specific strength; unfortunately, their poor toughness and corrosion resistance restrict their applications. Importantly, aluminum alloys have complementary toughness and corrosion resistance to magnesium alloys. Bonding Mg/Al dissimilar alloys can thus improve energy conservation and reduce emissions [1–3]. Therefore, Mg/Al dissimilar alloys joining is an important research topic. However, the most challenging problem in joining Mg/Al dissimilar alloys is the inevitable generation of brittle intermetallic compounds (IMC) in the joints like $Al_{12}Mg_{17}$ and Al_3Mg_2 [4–6]. Scholars have used friction stir welding (FSW) [7–9], diffusion

bonding [10–13], compound casting [14–16], and other methods [17,18] joining Mg/Al dissimilar alloys to overcome this problem. However, it is difficult to avoid the generation of brittle $Al_{12}Mg_{17}$ and Al_3Mg_2 IMC due to the limitations of these joining methods [19–21]. For example, some scholars found that the temperature of stir zone in the joints will rise (435 °C) due to the plastic deformation in FSW, resulting in constitutional liquation, which made it difficult to avoid the formation of $Al_{12}Mg_{17}$ and Al_3Mg_2 . The reaction layer of Mg–Al binary IMCs was reduced at lower welding temperature via diffusion bonding, but the generation of $Al_{12}Mg_{17}$ and Al_3Mg_2 cannot be completely avoided due to the high activity of Mg and Al elements [19]. Some scholars increase the shear strength of Mg/Al dissimilar joints by increasing the holding time via adding zinc coating

during diffusion bonding. Under the long-term insulation condition, the shear strength of the joints can only up to 30 MPa due to the formation of $\text{Al}_{12}\text{Mg}_{17}$ and Al_3Mg_2 [10]. Ultrasonic-assisted brazing was widely used in the joining of dissimilar alloys, such as Cu/Al dissimilar alloys and Ti/Al dissimilar alloys [22,23]. In this method, cavitation effect was introduced to break the oxide film on the surface of BMs, as so to realize the medium- and low-temperature and flux-free bonding in air [24–26]. Therefore, ultrasonic-assisted brazing was expected to join Mg/Al dissimilar alloys via some auxiliary means to overcome the difficulty of forming Mg–Al binary IMCs.

Adding interlayers is an effectively auxiliary method to control the generation of Al_3Mg_2 and $\text{Al}_{12}\text{Mg}_{17}$ IMC when joining Mg/Al dissimilar alloys. There are currently two types of interlayers. One is the single-interlayer that acts as a “physical barrier” for the contact of Mg/Al dissimilar alloys to avoid the generation of Al_3Mg_2 and $\text{Al}_{12}\text{Mg}_{17}$. When single-interlayer was used, there were few kinds of IMCs formed in the joints, and these IMCs were generally only binary phases, thus resulting in the general mechanical performance of the joints. For example, LI et al [27] used pure tin foil as the interlayer to join Mg/Al dissimilar alloys. Mg_2Sn IMC was generated in the joints to avoid the generation of Al_3Mg_2 and $\text{Al}_{12}\text{Mg}_{17}$. The shear strength of the joints was 60 MPa. GU et al [28] used zinc foil to join Mg/Al dissimilar alloys. Mg–Zn IMC was generated in the joints with a maximum shear strength of 57.62 MPa. The other is the multi-interlayer that puts the aluminum foils in direct contact with the Mg base metal (BM) to transform the reactants from Mg–Al binary IMC such as Al_3Mg_2 and $\text{Al}_{12}\text{Mg}_{17}$ into Mg–Al–X (X is generally the foil in contact with the aluminum foil in the multi-interlayer) ternary IMC. These ternary IMCs often have smaller Gibbs free energy such as the Mg–Al–Zn ternary phase [3]. These ternary IMCs reinforce the mechanical performance of the joints. For example, ZHANG et al [29] used Al/Ni multi-interlayer to join Mg/Al dissimilar alloys. Mg–Al–Ni ternary IMCs were formed in the joints, which increased the shear strength of the joints from 19.5 MPa using Ni single interlayer with the Mg_2Ni and Al_3Ni IMCs, to 25.8 MPa. PENG et al [30] used multi-interlayer composed of Al/Zn/Ni to join Mg/Al dissimilar alloys. Mg–Al–

Zn ternary IMCs were generated in the joints, which markedly enhances the bonding between Ni foil and base metals (BMs). Thus, the shear strength of the joints was increased from 21.2 MPa by using pure Ni interlayer with the formation of Mg_2Ni and Al_3Ni IMCs, to 95.3 MPa [30,31].

To date, copper foil interlayers have been widely used for joining dissimilar alloys and are expected to have potential in ultrasonic-assisted brazing of Mg/Al dissimilar alloys [32–34]. Copper foil can act as a “physical barrier” to avoid the generation of Al_3Mg_2 and $\text{Al}_{12}\text{Mg}_{17}$. The Al_2Cu formed at the Al/Cu interface enhanced the bonding of interface [35]. In addition, zinc foils were added between copper foil and BMs in consideration of the cavitation effect that can break the oxide film on the BMs after the zinc liquid wetting the surface of BMs. This promoted significant amounts of Mg and Al atoms to diffuse to the brazing seam and react with copper foil, as so to enhance the bonding between Cu interlayer and BMs. On this basis, Al/Zn/Cu/Zn multi-interlayers were used for ultrasonic-assisted brazing of MB8/2024 dissimilar alloys in air. Here, the evolution of IMCs in the joints was investigated and its influence on mechanical properties of joints was analyzed.

2 Experimental

The alloys used in this work were 2024 aluminum alloy (3.8–4.7 wt.% Cu, 1.2–1.8 wt.% Mg, 0.5 wt.% Fe, 0.5 wt.% Si, 0.3 wt.% Zn, and 0.15 wt.% Ti) and MB8 magnesium alloy (1.3–2.2 wt.% Mn, 0.3 wt.% Zn, 0.2 wt.% Al, and 0.15–0.35 wt.% Ce) with sizes of 20 mm × 20 mm × 3 mm. The thicknesses of the Cu foil, zinc foil, and aluminum foil in the test were 100, 50, and 50 μm, respectively; the corresponding sizes of the foils were 30 mm × 30 mm, 20 mm × 20 mm, and 20 mm × 20 mm, respectively. The BMs were treated with 400[#], 800[#], and 1200[#] emery papers and ultrasonically cleaned in ethanol for 15 min.

The ultrasonic-assisted brazing equipment was used for this test (Fig. 1(a)). The test was conducted in air with a constant pressure of 0.15 MPa. The ultrasonic power was set to be 1 kW and the frequency was 30 kHz. The ultrasonic amplitude was 12 μm. A contact thermometer (TES1310) was used to control the temperature of samples, which were heated via a medium frequency induction

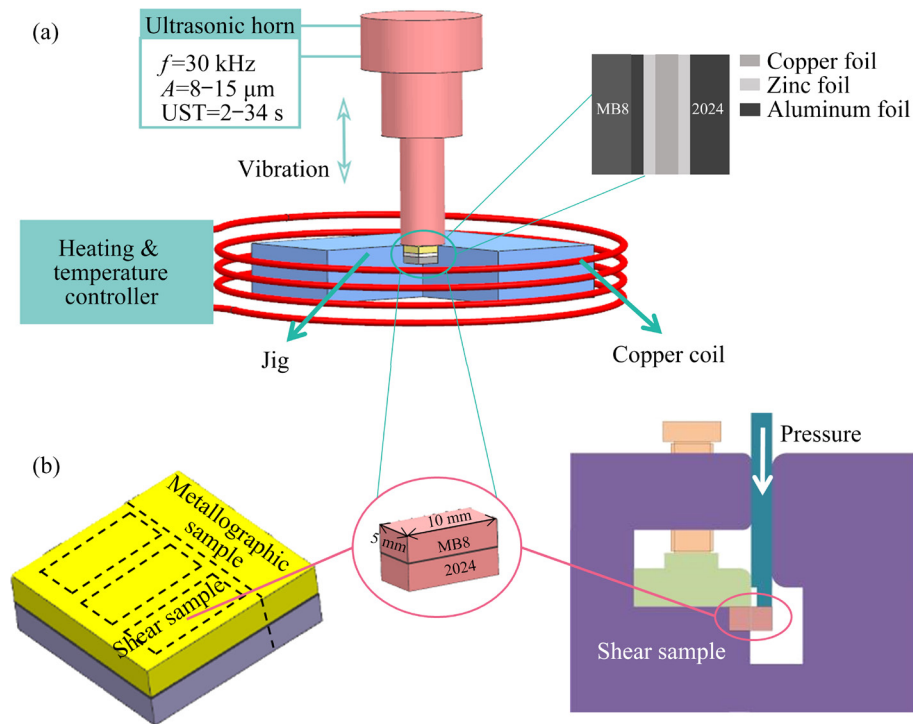


Fig. 1 Schematic of ultrasonic-assisted brazing and Al/Zn/Cu/Zn multi-interlayer (a); Schematic of metallographic sample, shear samples, and shear fixture (b)

furnace. At $400\text{ }^\circ\text{C}$, a series of ultrasonic treatment (UST) time was applied to the samples and then the samples were cooled in air.

The samples were sliced using an electrical discharge machine to fabricate metallographic and shear samples with sizes of $20\text{ mm} \times 8\text{ mm}$ and $10\text{ mm} \times 5\text{ mm}$, respectively (Fig. 1(b)). The microstructure and fracture path were observed using scanning electron microscope (JSM-7800F). Energy dispersive spectrometer (EDS, X-MaxN) was used to determine the chemical composition of each phase. The electron diffraction patterns were achieved via a focused ion beam scanning electron microscopy (FIB-SEM, FEI Strata 400S). Shear strength values of the joints were obtained by a tensile machine (WDW-50KN) with 0.1 mm/s loading speed. Three groups of samples were measured at each UST time. The IMCs on the surface of the fracture were detected via X-ray diffraction (Maxima XRD-7000). An Hysitron TI-PREMIER nano-indentation tester was used to determine the nano-indentation hardness and the elastic modulus. The testing was carried out at indentation depth of 500 nm for 10 s . Five sites were struck on every phase during nano-indentation. Two of the data points that were totally struck on

the phases were adapted to create the histogram of nano-indentation hardness and elastic modulus, and one of the data points was used to create load–displacement curves.

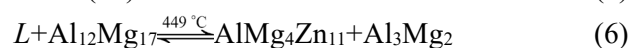
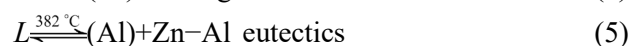
3 Results and discussion

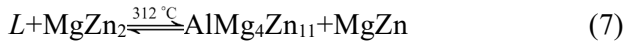
3.1 Microstructure evolution of joints with increasing UST time

The Zn–Al, and Al–Cu binary eutectic reactions (Eqs. (1) and (2)) occurred on the 2024 side with the formation of $\alpha(\text{Al})$, $\eta\text{-Zn}$, and Al_2Cu . These reactants enhanced the Al–Cu bonding interface [35]. The microstructures on the 2024 side had almost no change in the test, and thus the microstructure evolution on the MB8 side of the joints is the main focus here.



The main reactions on the MB8 side using Al/Zn/Cu/Zn multi-interlayer were





The evolution of IMCs in the joints by using Al/Zn/Cu/Zn multi-interlayer with increasing UST time is shown in Fig. 2. The EDS analysis results of possible phases in Fig. 2 are listed in Table 1. There is no defect in the joints in the ultrasonic range

under the test conditions used here. Therefore, using Al/Zn/Cu/Zn multi-interlayers can effectively bond MB8/2024 dissimilar alloys at 400 °C in air. The ultrasonic vibration can increase the dislocation density and accelerate the diffusion and reaction of atoms; the microstructure in the joints changed accordingly with UST time [36].

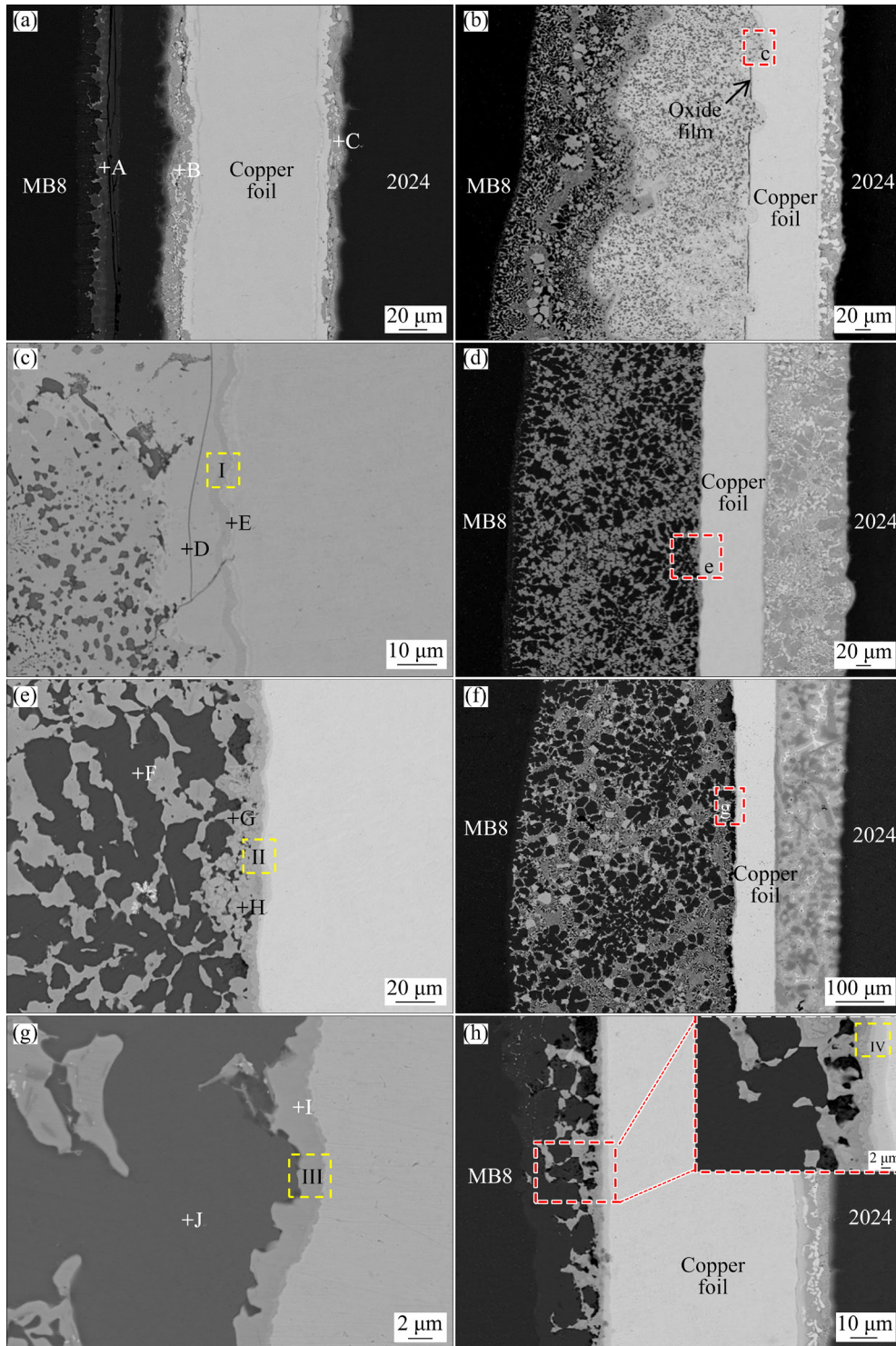


Fig. 2 Microstructure of joints by using Al/Zn/Cu/Zn multi-interlayer at 400 °C: (a) 2 s; (b, c) 4 s; (d, e) 14 s; (f, g) 22 s; (h) 34 s

Table 1 Chemical composition and possible phases of different regions in Fig. 2

UST time/s	Point	Chemical composition/at.%				Possible phase
		Al	Mg	Zn	Cu	
2	A	58.06	39.53	2.15	0.26	Al ₃ Mg ₂
	B	10.47		58.83	30.71	Zn–Al eutectics + Cu ₅ Zn ₈
	C	50.24		42.43	7.33	Zn–Al eutectics
4	D	13.88	15.25	56.36	14.51	Mg–Al–Zn–Cu mixture + η -Zn
	E	16.46	14.37	36.48	32.69	Al–Mg–Zn–Cu mixture
14	F	5.11	92.73	2.15		α -Mg
	G	36.94	37.30	19.03	6.73	Mg–Al–Zn mixture
	H	66.71	0.45	2.73	30.11	Al ₂ Cu
22	I	22.06	36.87	15.89	25.18	Al–Mg–Zn–Cu mixture
	J	1.52	97.08	1.39		α -Mg

With 2 s UST (Fig. 2(a)), Zn–Al and Zn–Cu eutectic reactions occurred on the Al/Cu interface on Mg BM side with the generation of Zn–Al eutectics and Cu₅Zn₈ (Region B), and the Zn–Al eutectic reaction occurred on the 2024 side with the generation of Zn–Al eutectics (Region C). However, the aluminum foil on the MB8 side did not completely dissolve due to insufficient reaction, which hindered the contact and reaction between Mg and Zn atoms; thus Al₃Mg₂ (Region A), a brittle intermetallic compound (IMC), was produced, which harms the joints.

With 4 s UST (Fig. 2(b)), the aluminum foil completely dissolved. Mg–Al and Al–Zn eutectic reactions occurred in the brazing seam with the formation of a eutectic liquid phase; this in turn promoted the diffusion of Mg atoms from MB8 to the brazing seam, thus resulting in an expansion of the reaction area. However, there was a regional stratification phenomenon due to the insufficient UST, which made inter-diffusion of Mg and Zn atoms inadequate. The light gray layer near the copper foil was mainly a mixture of Al, Mg, Zn, and Cu; the dark gray layer was Al₃Mg₂ that was not completely transformed into the ternary phase. Semicircular corrosion pits with similar sizes were locally generated along the surface of Cu foil via ultrasonic cavitation [37–39]. Oxide film on the surface of corrosion pits was shattered due to cavitation effect, and its fragments were scattered in the brazing seam, while a black oxide film remained on the surface of Cu foil far from the corrosion pits. The corrosion pits caused a large

fluctuation in the width of the remaining Cu interlayer (Fig. 3(a)), and there was a significant reduction in value. A uniform IMC reaction layer (Region E) along the surface of Cu interlayer on MB8 side could be observed in the local enlarged view of corrosion pits (Fig. 2(c)). The EDS analysis results showed that the reactant in this layer was a mixture composed of Al, Mg, Zn, and Cu. In addition, Zn–Al eutectic reaction occurred on the Zn/Al interface, thus forming η -Zn (Region D).

With 14 s UST (Fig. 2(d)), the regional stratification phenomenon on the MB8 side disappeared due to the full inter-diffusion of Mg and Zn atoms. The Mg–Al–Zn mixtures (Region G) and granular phase of α -Mg (Region F) were evenly distributed in the joints. A continuously distributed IMC layer was also observed on the surface of Cu interlayer (Fig. 2(e)), and the dispersed Al₂Cu particles (Region H) were close to this IMC layer.

With 22 s UST (Fig. 2(f)), the average width of the brazing seam on the MB8 side reached a maximum (Fig. 3(b)), about 460.59 μ m. Sufficient UST made the MB8 and interlayers fully melt and react, thus resulting in the generation of a large number of dispersed massive α -Mg phases in the brazing seam. An IMCs layer on the surface of Cu interlayer was also observed (Fig. 2(g)). EDS results showed that this IMCs layer was a mixture composed of Al, Mg, Zn, and Cu elements (Region I), combined with solid solution α -Mg (Region J).

With 34 s UST (Fig. 2(h)), the liquid metal was squeezed out of the brazing seam in large

quantities because it was too soft to support the ultrasonic pressure [36]. The average width of the remaining Cu interlayer was the smallest, only about 71.26 μm (Fig. 3(a)). And the average width of the brazing seam on the MB8 side was obviously reduced, only about 31.44 μm (Fig. 3(b)). However, there was still an IMCs layer on the surface of Cu interlayer.

3.2 Fracture path

Figure 4 shows the morphologies and XRD patterns of the fracture path for joints prepared with 4 s, 14 s and 22 s UST. As shown in Figs. 4(a–c), the joints were all broken on the IMCs layer. The

XRD patterns (Figs. 4(d–f)) confirm that the IMC on the surface of fracture was a mixture of $\text{AlMg}_4\text{Zn}_{11}$, Al_2Cu , and Al_3Mg_2 with 4 s UST. The IMC on the surface of fracture was a mixture of $\text{AlMg}_4\text{Zn}_{11}$, $\text{Al}_5\text{Mg}_{11}\text{Zn}_4$, Al_3Mg_2 , and Al_2Cu with 14 s UST. The IMC on the surface of fracture was a mixture of $\text{AlMg}_4\text{Zn}_{11}$, CuMgZn , and $\text{Al}_5\text{Mg}_{11}\text{Zn}_4$ with 22 s UST. Al_3Mg_2 in the joints were completely transformed into Mg–Al–Zn ternary phases as UST time was increased to 22 s. This is because the reaction in the brazing seam was sufficient with 22 s UST. Al_2Cu that was expected to play a role of reinforcing phase fully dissolved with Cu_5Zn_8 on the surface of Cu interlayer after

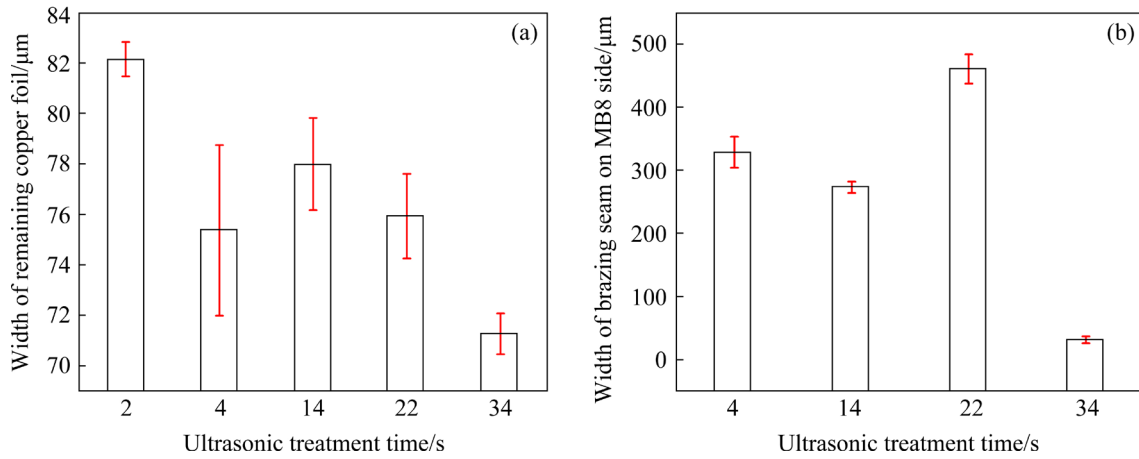


Fig. 3 Width of remaining copper foil (a) and width of brazing seam on MB8 side (b)

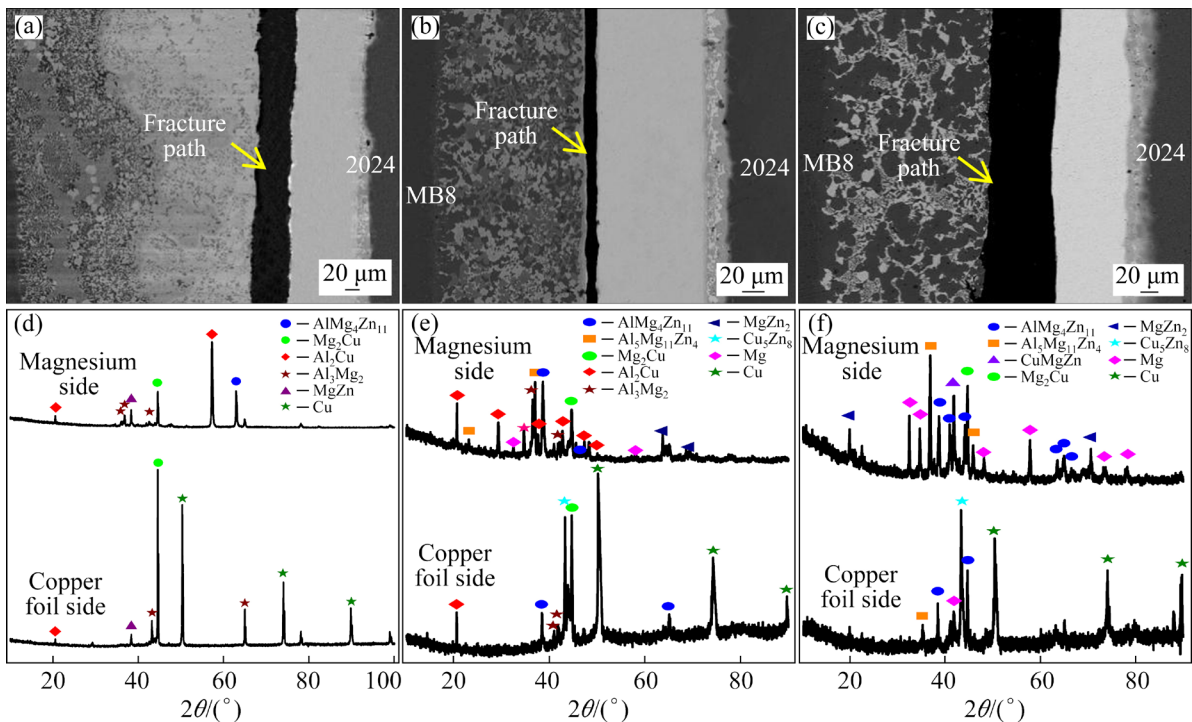


Fig. 4 Morphologies (a–c) and XRD patterns (d–f) of fracture path with UST: (a, d) 4 s; (b, e) 14 s; (c, f) 22 s

diffusion of Mg atoms. The reactants were then transformed into Cu–Mg–Zn ternary IMC. The evolution of IMC layer on the surface of Cu interlayer was caused by the sufficient inter-diffusion and reactions of atoms with increasing UST time, which in turn promoted the transformation.

3.3 Calibration of IMC layer by TEM

Figure 5 shows TEM images of the IMCs at different UST time; the sampling positions corresponded to I, II, III, and IV in Fig. 2. The calibration results of 4 s UST were consistent with the XRD analysis (Figs. 5(a–c)). The IMCs layer was the mixture of Al_2Cu , $\text{AlMg}_4\text{Zn}_{11}$, Al_3Mg_2 , and MgZn .

An interesting phenomenon occurred in 14 s UST (Fig. 6). Quasicrystals were found in the IMCs layer expect the $\text{AlMg}_4\text{Zn}_{11}$ phase. This reactant was considered to be a quasicrystal of the system composed of Al, Mg, Zn, and Cu based on the elements distribution in the region where the quasicrystal was located. The electron diffraction pattern shown in Fig. 6(a) suggests that the quasicrystal was a decagonal quasicrystal. Fourier transform (FFT) of its high-resolution picture (Fig. 6(g)) shows diffraction spots in Fig. 6(h). These observations proved that it is decagonal quasicrystal. The inverse FFT in Fig. 6(i) shows that the distance between two adjacent quasicrystals that was calibrated according to the parallel symmetry of quasicrystals were 0.96 and 1.163 nm, respectively. The growth direction of the different crystal planes was different, and thus the crystal plane spacing was also different [40]. BOKHONOV et al [41] found that the crystal plane spacing of the (110) plane of Frank–Kasper (F–K) phase $\text{Mg}_{32}(\text{Al},\text{Zn})_{49}$ is about 1.01 nm, which is quite close to our calibration distances. Therefore, we believe that the quasicrystal in this test is $\text{Mg}_{32}(\text{Al},\text{Zn})_{49}$. Quasicrystals can be prepared not only by mature processes such as valence electron concentration, but also by rapid solidification technology [42,43]. At present, no quasicrystals were found in the ultrasonic-assisted brazing dissimilar alloys. We think that the formation of quasicrystals was related to the cavitation effect. The molten liquid alloys could produce bubbles under cavitation effect during the brazing process. These bubbles could rapidly collapse when the

external pressure was higher than the internal pressure. As a result, the joints experienced a localized and rapid increase in temperature and pressure. Therefore, there was a rapid cooling process [37–39], and the quasicrystal appeared due to the short and rapid cooling process of molten liquid alloys during solidification. These quasicrystals were considered to be metastable quasicrystals according to their grain size. The rapid cooling process in solidification was very short, and the transformation from quasicrystal to single crystal was not completed; thus, it was present in the joints in the form of a quasicrystal [44].

With 22 s UST, the IMCs layer was calibrated as a mixture of $\text{AlMg}_4\text{Zn}_{11}$, MgZnCu , Cu_5Zn_8 , and Mg_2Cu (Figs. 5(e–h)). The molten aluminum foil and zinc foil completely wetted the MB8 BMs due to the adequate ultrasonic action. This in turn led to Mg–Al–Zn and Mg–Zn–Cu ternary eutectic reactions in the brazing seam with the generation of $\text{AlMg}_4\text{Zn}_{11}$ and MgZnCu IMCs.

With 34 s UST, there was still an IMCs layer on the surface of Cu interlayer, although a large amount of liquid phase was extruded. This IMCs layer was calibrated as a mixture of Mg_2Cu , MgZn_2 , and Cu_5Zn_8 (Figs. 5(i, j)) by TEM. There was no IMC containing Al with 34 s UST, because the molten Al liquid phase was basically extruded via ultrasonic vibration.

Experiments show that the use of multi-interlayers is conducive to the transformation from binary phase into ternary phase. The ternary IMC of the Mg–Al–Zn system is considered to be the reinforcing phase in Mg/Al dissimilar alloys, and scholars have verified the role of $\text{AlMg}_4\text{Zn}_{11}$ in strengthening the mechanical properties of the Mg/Al joints [30]. Ultrasonic action affects the composition of the IMCs layer by promoting the reaction in the brazing seam, which in turn affects the mechanical performance of the joints according to the microstructure evolution of the brazing seam in the joints. Therefore, we attribute the change of mechanical properties of the joints to the IMCs layer that evolve with UST time.

3.4 Thermodynamic analysis

The excess Gibbs free energy of binary systems ($\Delta G_{\text{Al,Mg}}$, $\Delta G_{\text{Zn,Al}}$, $\Delta G_{\text{Zn,Mg}}$) at 400 °C was calculated via the Miedema model, as shown in Fig. 7(a). Obviously, values of $\Delta G_{\text{Zn,Al}}$ were positive

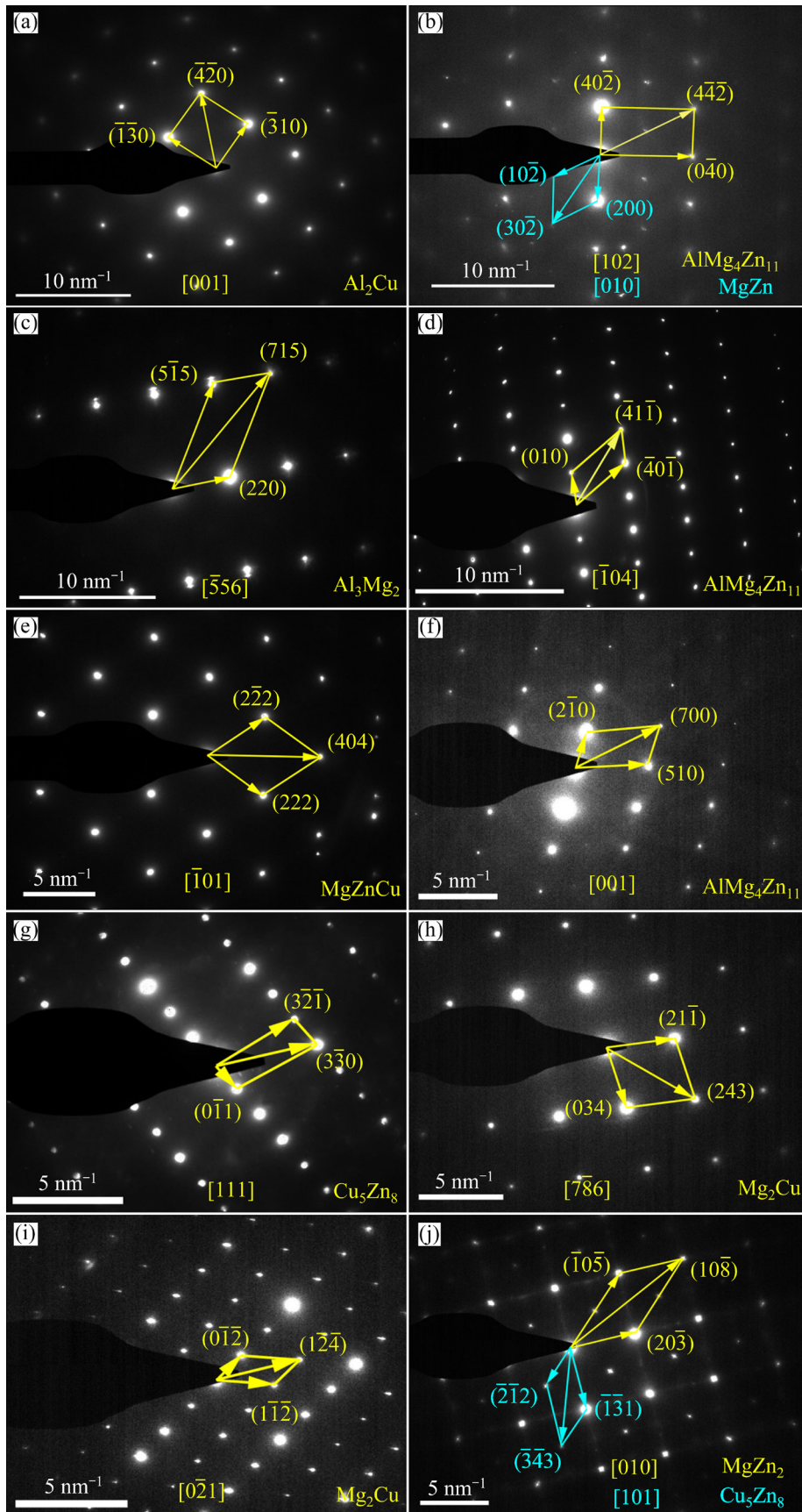


Fig. 5 Electron diffraction patterns at IMC layer along Cu interlayer: (a–c) Area I in Fig. 2(c); (d) Area II in Fig. 2(e); (e–h) Area III in Fig. 2(g); (i, j) Area IV in Fig. 2(h)

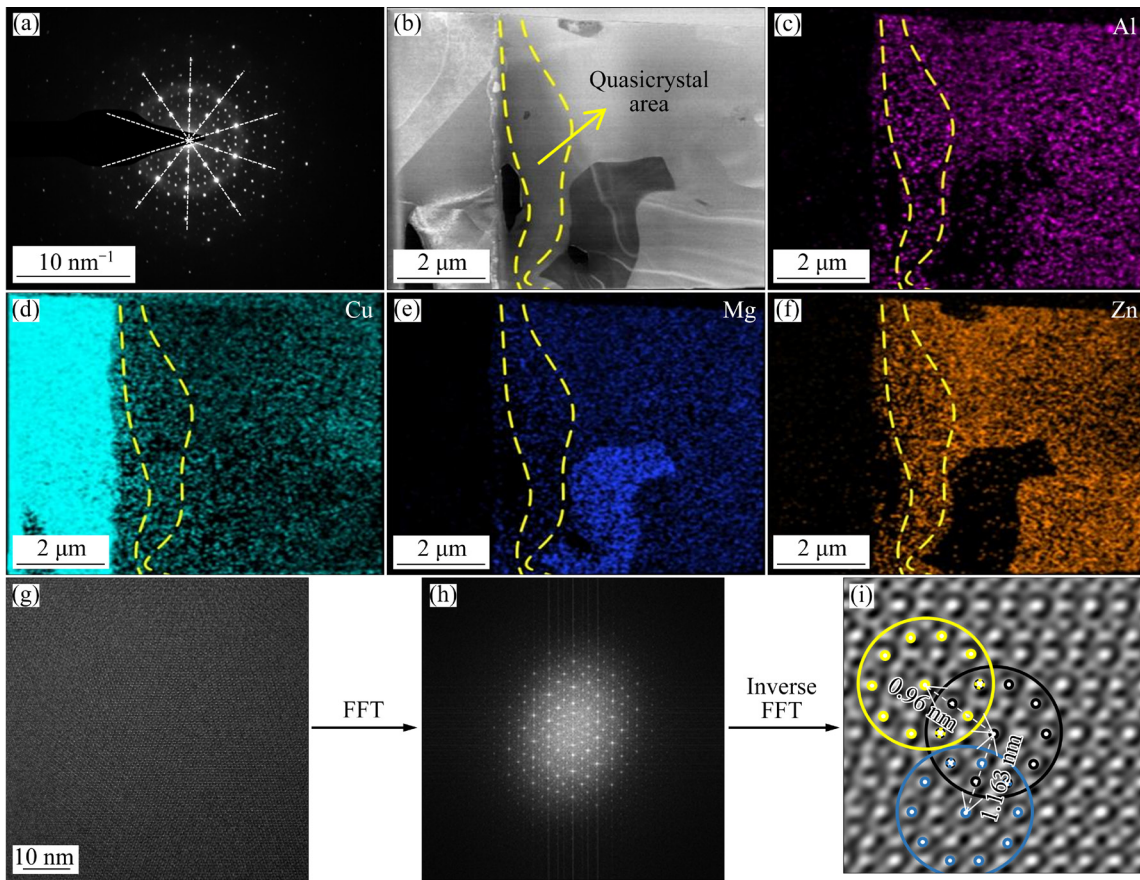


Fig. 6 Electron diffraction pattern (a); Element distribution of quasicrystal area (b–f); High-resolution image (g), FFT of high-resolution image (h) and inverse FFT of high-resolution image (i)

while values of $\Delta G_{\text{Al,Mg}}$ and $\Delta G_{\text{Zn,Mg}}$ were negative. This suggests that there was no spontaneous reaction between Zn and Al while the generation of Al_3Mg_2 and MgZn in the brazing seam was due to the spontaneous reaction between Al and Mg as well as Mg and Zn. The values of $\Delta G_{\text{Al,Mg}}$ were the lowest, which indicated that the reaction forming Mg–Al IMC was the most favorable. Therefore, Al_3Mg_2 , with a smaller Gibbs free energy, was the main reactant in the joints.

The systems became ternary systems ($\Delta G_{\text{Mg,Al,Zn}}$) when the aluminum foil cannot block the reaction between Mg and Zn. The Gibbs free energy of the Mg–Al–Zn ternary was calculated via the Toop model (Fig. 7(b)) to reveal the reaction tendency among Mg, Al, and Zn elements. According to the principle [44–47], Mg was selected as an asymmetric component in the calculation of $\Delta G_{\text{Mg,Al,Zn}}$. The values of $\Delta G_{\text{Mg,Al,Zn}}$ at $400 \text{ }^\circ\text{C}$ were always negative, which suggested that there was always a spontaneous reaction in the Mg–Al–Zn ternary systems. The ternary phase with the lowest $\Delta G_{\text{Mg,Al,Zn}}$ in this system was considered

to be $\text{AlMg}_4\text{Zn}_{11}$ (-38.65 kJ/mol); the $\Delta G_{\text{Mg,Al,Zn}}$ of Al_3Mg_2 IMC in this system was -31.94 kJ/mol . These results show that $\text{AlMg}_4\text{Zn}_{11}$ IMC is most easily formed in this system, and a thermodynamic basis is provided for transformation of Al_3Mg_2 IMC into $\text{AlMg}_4\text{Zn}_{11}$ IMC in the brazing seam.

The chemical potential in the ternary system explains the driving force in the reaction process (Figs. 7(c–e)). The chemical potentials of Al (μ_{Al}) at the composition points of Mg and Zn were both about -46.50 kJ/mol . The chemical potentials of Mg (μ_{Mg}) at the composition points of Al and Zn were about -58.80 and -66.60 kJ/mol , respectively. The chemical potentials of Zn (μ_{Zn}) at the composition points of Mg and Al were about -55.68 and -51.75 kJ/mol , respectively. Therefore, there was a more obvious mutual diffusion trend between Mg and Zn in the process of elements diffusion and reaction. The diffusion trends of Al to Mg and Zn were basically the same. During bonding, the aluminum foil hindered the interdiffusion between Mg and Zn, and Al_3Mg_2 was formed in the brazing seam when the aluminum foil

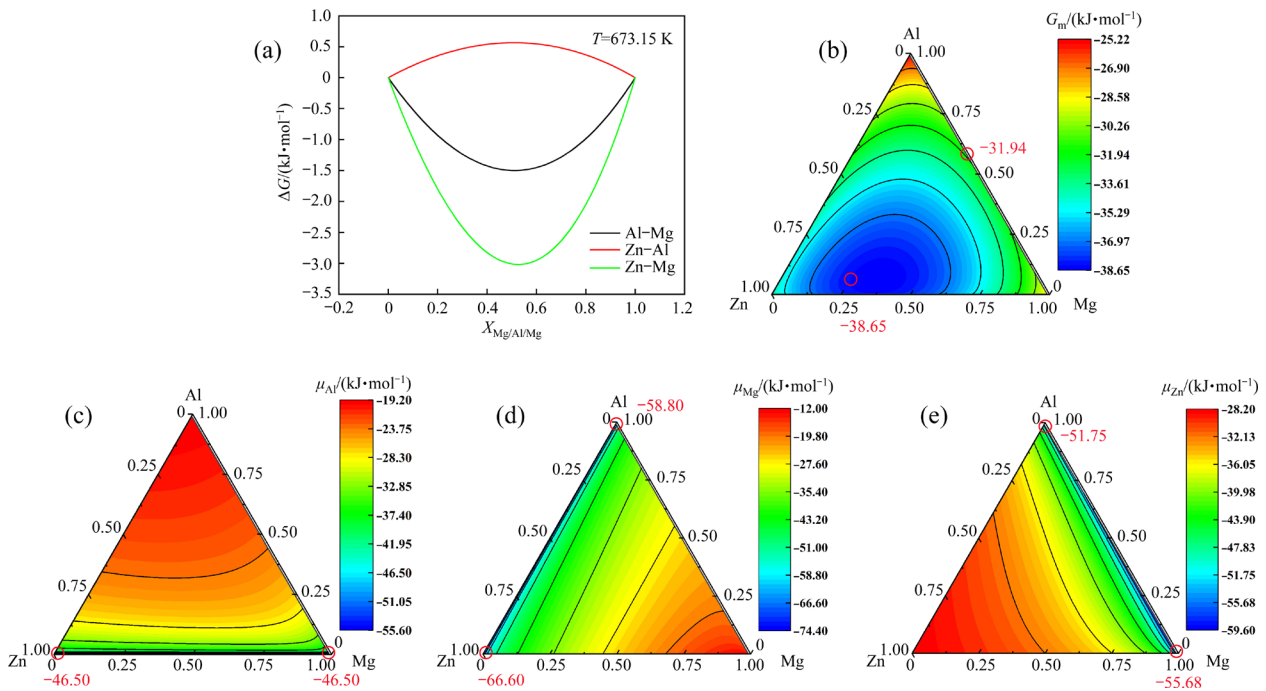


Fig. 7 Calculated $\Delta G_{\text{Al,Mg}}$, $\Delta G_{\text{Zn,Al}}$, and $\Delta G_{\text{Zn,Mg}}$ at 400 °C (a); Calculated $\Delta G_{\text{Mg,Al,Zn}}$ at 400 °C (b); Calculated chemical potentials of Al, Mg, and Zn (μ_{Al} , μ_{Mg} , and μ_{Zn}) at 400 °C (c–e)

did not dissolve. The reaction in the joints became sufficient with longer UST time. This in turn led to a reaction among Mg, Al, and Zn with transformation of the IMC in the brazing seam from Al_3Mg_2 into $\text{AlMg}_4\text{Zn}_{11}$.

3.5 Mechanical performance of joints

The nano-indentation hardness and elastic modulus of the IMCs layer and the nano-indentation load–displacement curves with different UST time by using the Al/Zn/Cu/Zn multi-interlayer are shown in Fig. 8. Obviously, with 4 s UST, $\text{Al}_2\text{Cu} + \text{AlMg}_4\text{Zn}_{11} + \text{Al}_3\text{Mg}_2 + \text{MgZn}$ IMC layer had the highest hardness of 2.38–2.633 GPa with elastic modulus of 37.7–38.94 GPa. The hardness of $\text{AlMg}_4\text{Zn}_{11} + \text{Mg}_{32}(\text{Al,Zn})_{49}$ quasicrystal IMC layer with 14 s UST was 1.51–1.94 GPa with elastic modulus of 35.51–38.95 GPa. The hardness of $\text{AlMg}_4\text{Zn}_{11} + \text{MgZnCu} + \text{Cu}_5\text{Zn}_8 + \text{Mg}_2\text{Cu}$ IMC layer with 22 s UST was the lowest (1.22–1.36 GPa) and the elastic modulus was 31.96–34.56 GPa. The change of shear strength with UST time is shown in Fig. 9(a). Figure 9(b) shows the shear load–displacement curves with different UST time. The shear strength peaked at 22 s UST (85.26 MPa). This was because the Mg–Al and Al–Cu binary phases in the joints on Mg BM side were fully transformed into ternary phases under sufficient

reaction. The $\text{AlMg}_4\text{Zn}_{11}$ and MgZnCu , as main reinforcing phases, were formed in the IMCs layer. They combined with bulk α -Mg, leading to optimal mechanical performance of the joints.

However, the mechanical performance of the joints was worse due to incomplete dissolution of aluminum foil when the UST time was less than 22 s. This was because the Mg–Al eutectic reaction occurred at the Mg/Al interface at the beginning of dissolution of aluminum foil with the formation of Al_3Mg_2 , a brittle IMC that destroys the mechanical performance of joints. And the eutectic reactions at the Zn/Al interface to form η -Zn and $\alpha(\text{Al})$ were insufficient. Furthermore, the insufficient dissolution and diffusion of Mg atoms led to less α -Mg solid solution in the brazing seam. This was not enough to improve the mechanical performance of joints. Specifically, when the UST time was 4 s, the IMCs layer only existed where the corrosion pits appeared. This discontinuity also had an adverse impact on the mechanical performance of the joints. The mechanical performance of the joints was not enhanced when the UST time was 14 s because the quasicrystal was hard and brittle at room temperature [48] and it distributed in the IMC layer in the sheet form. When the UST time was over 22 s, the dissolved aluminum was squeezed out of the brazing seam, resulting in a large number

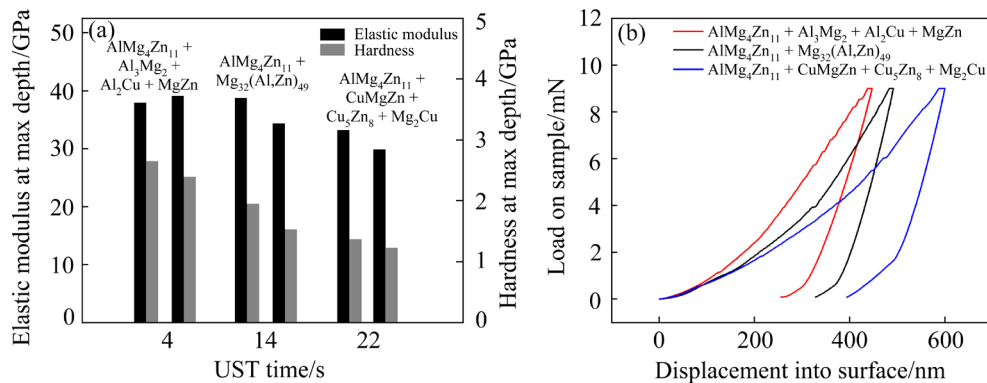


Fig. 8 Nano-indentation hardness and elastic modulus (a), and load–displacement curves (b) of phase formed along copper foil at Mg BM side on cross-section of joints

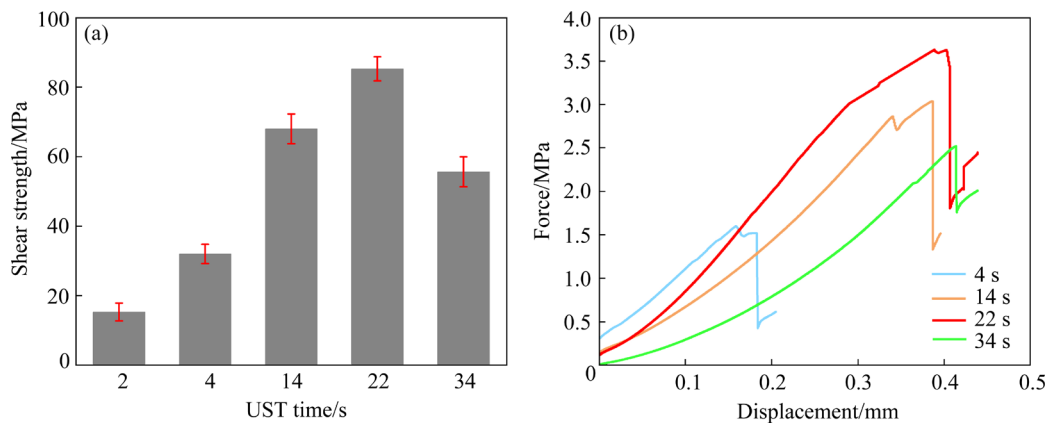


Fig. 9 Shear strength of joints at different UST time (a), and force–displacement curves (b)

of Mg atoms contacting and reacting with Zn and Cu atoms with the formation of the brittle $MgZn_2$ and Mg_2Cu IMC [49], which increased the brittleness of the joints and reduced the mechanical performance of the joints.

In conclusion, the mechanical properties of the joints was closely related to the IMCs layer on the surface of Cu interlayer on MB8 side. Therefore, the composition of this IMC layer can be controlled by adjusting the UST time, which impacts the reaction in the brazing seam. One can also change the set-up of the multi-interlayer to obtain a joint with the required mechanical performance.

4 Conclusions

(1) MB8/2024 dissimilar alloys by using Al/Zn/Cu/Zn multi-interlayers could achieve defect-free joining at 400 °C in air, and an IMC layer was formed along the Cu interlayer on the MB8 side, which changed from $Al_2Cu + AlMg_4Zn_{11} + Al_3Mg_2 + MgZn$ (4 s) to $AlMg_4Zn_{11} + Mg_{32}(Al,Zn)_{49}$

quasicrystal (14 s), to $AlMg_4Zn_{11} + MgZnCu + Cu_5Zn_8 + Mg_2Cu$ (22 s), and to $Mg_2Cu + MgZn_2 + Cu_5Zn_8$ (34 s) with increasing ultrasonic treatment (UST) time. At each UST time, the joints fractured along this IMC layer.

(2) An $Mg_{32}(Al, Zn)_{49}$ quasicrystal was found in the ultrasonic-assisted brazing MB8/2024 for the first time because of the rapid cooling process due to ultrasonic cavitation.

(3) The thermodynamic analysis shows that the $\Delta G_{Mg,Al,Zn}$ of $AlMg_4Zn_{11}$ was the smallest (−38.65 kJ/mol) and provided the basis for transformation from Mg–Al binary IMCs into Mg–Al–Zn ternary IMC.

(4) The shear strength of the joints peaked at 85.26 MPa when the ultrasonic treatment time was 22 s.

Acknowledgments

This project was supported by the National Natural Science Foundation of China (Nos. 51871128, 51875300), the Natural Science

Foundation of Shandong Province, China (No. ZR2018MEE017), Local Science and Technology Development Projects Guided by the Central Government, China (No. YDZX20203700003578) and 2021 Major Industrial Key Project of Transformation of Old and New Driving Forces in Shandong Province, China.

References

- [1] ZHAO Ying, PEI Jiu-yan, GUO Li-li, YUN Xin-bing, MA Huai-chao. Effects of extrusion speed of continuous extrusion with double billets on welding performance of 6063 Al alloy [J]. Transactions of Nonferrous Metals Society of China, 2021, 31(6): 1561–71.
- [2] ZHANG Zheng, JIANG Wen-ming, LI Guang-yu, WANG Jun-long, GUAN Feng, JIE Guo-liang, FAN Zi-tian. Improved interface bonding of Al/Mg bimetal fabricated by compound casting with Nd addition [J]. Materials Science and Engineering A, 2021, 826: 141998.
- [3] XU Nan, ZHANG Wei-da, CAI Si-qi, ZHOU Yue, SONG Qi-ning, BAO Ye-feng. Microstructure and tensile properties of rapid-cooling friction-stir-welded AZ31B Mg alloy along thickness direction [J]. Transactions of Nonferrous Metals Society of China, 2020, 30(12): 3254–62.
- [4] LIU Wen-sheng, LONG LU-ping, MA Yun-zhu, WU Lei. Microstructure evolution and mechanical properties of Mg/Al diffusion bonded joints [J]. Journal of Alloys and Compounds, 2015, 643: 34–39.
- [5] BINOTSCH C, NICKEL D, FEUERHACK A, AWISZUS B. Forging of Al–Mg compounds and characterization of interface [J]. Procedia Engineering, 2014, 81: 540–545.
- [6] AZIZI A, ALIMARDAN H. Effect of welding temperature and duration on properties of 7075 Al to AZ31B Mg diffusion bonded joint [J]. Transactions of Nonferrous Metals Society of China, 2016, 26(1): 85–92.
- [7] LAKSHMINARAYANAN A K, ANNAMALAI V E. Fabrication and performance evaluation of dissimilar magnesium–aluminium alloy multi-seam friction stir clad joints [J]. Transactions of Nonferrous Metals Society of China, 2017, 27(1): 25–35.
- [8] ZHAO Jun-jie, WU Chuan-song, SU Hao. Acoustic effect on the tensile properties and metallurgical structures of dissimilar friction stir welding joints of Al/Mg alloys [J]. Journal of Manufacturing Processes, 2021, 65: 328–341.
- [9] JAYARAJ R K, MALARVIZHI S, BALASUBRAMANIAN V. Electrochemical corrosion behaviour of stir zone of friction stir welded dissimilar joints of AA6061 aluminium–AZ31B magnesium alloys [J]. Transactions of Nonferrous Metals Society of China, 2017, 27(10): 2181–2192.
- [10] GOLDEN RENJITH NIMAL R J, CHENTHIL M, SANGAMAESWARAN R, HARIHARAN R, ESAKKIMUTHU G. An investigation on microstructural evolution and mechanical properties of Zn coating as interlayer on Mg–Al alloys using diffusion bonding [J]. Materials Today: Proceedings, 2021, 46: 3512–3516.
- [11] DING Yun-long, WANG Jian-gang, ZHAO Ming, JU Dong-ying. Effect of annealing temperature on joints of diffusion bonded Mg/Al alloys [J]. Transactions of Nonferrous Metals Society of China, 2018, 28(2): 251–258.
- [12] SEYYED AFGHAHI S S, JAFARIAN M, PAIDAR M, JAFARIAN M. Diffusion bonding of Al 7075 and Mg AZ31 alloys: Process parameters, microstructural analysis and mechanical properties [J]. Transactions of Nonferrous Metals Society of China, 2016, 26(7): 1843–1851.
- [13] ZHAO L M, ZHANG Z D. Effect of Zn alloy interlayer on interface microstructure and strength of diffusion-bonded Mg–Al joints [J]. Scripta Materialia, 2008, 58(4): 283–286.
- [14] ZHANG Zheng, JIANG Wen-ming, LI Guang-yu, WANG Jun-long, GUAN Feng, JIE Guo-liang, FAN Zi-tian. Effect of La on microstructure, mechanical properties and fracture behavior of Al/Mg bimetallic interface manufactured by compound casting [J]. Journal of Materials Science & Technology, 2022, 105: 214–225.
- [15] LI Guang-yu, JIANG Wen-ming, GUAN Feng, ZHU Jun-wen, YU Yang, FAN Zi-tian. Effect of different Ni interlayers on interfacial microstructure and bonding properties of Al/Mg bimetal using a novel compound casting [J]. Journal of Manufacturing Processes, 2020, 50: 614–628.
- [16] WANG Jun-long, GUAN Feng, JIANG Wen-ming, LI Guang-yu, ZHANG Zheng, FAN Zi-tian. The role of vibration time in interfacial microstructure and mechanical properties of Al/Mg bimetallic composites produced by a novel compound casting [J]. Journal of Materials Research and Technology, 2021, 15: 3867–3879.
- [17] GAO Lei, LI Feng, WANG Ye, XIAO Xing-mao, HUO Peng-da. Fabrication and interface structural behavior of Mg/Al thickness-oriented bonding sheet via direct extrusion [J]. Metals and Materials International, 2022, 28: 1960–1970.
- [18] ZHANG Ting-ting, WANG Wen-xian, ZHANG Wei, WEI Yi, CAO Xiao-qing, YAN Zhi-feng, ZHOU Jun. Microstructure evolution and mechanical properties of an AA6061/AZ31B alloy plate fabricated by explosive welding [J]. Journal of Alloys and Compounds, 2018, 735: 1759–1768.
- [19] MOFID M A, LORYAEI E. Investigating microstructural evolution at the interface of friction stir weld and diffusion bond of Al and Mg alloys [J]. Journal of Materials Research and Technology, 2019, 8: 3872–387.
- [20] BANDI A, BAKSHI S R. Effect of pin length and rotation speed on the microstructure and mechanical properties of friction stir welded lap joints of AZ31B–H24 Mg alloy and AA6061–T6 Al alloy [J]. Metallurgical and Materials Transactions A, 2020, 51(12): 6269–6282.
- [21] SACHIN K, WU Chuan-song, SHI Lei. Intermetallic diminution during friction stir welding of dissimilar Al/Mg alloys in lap configuration via ultrasonic assistance [J]. Metallurgical and Materials Transactions A, 2020, 51: 5725–5742.
- [22] JI Hong-jun, CHEN Hao, LI Ming-yu. Effect of ultrasonic transmission rate on microstructure and properties of the ultrasonic-assisted brazing of Cu to alumina [J]. Ultrasonics Sonochemistry, 2017, 34: 491–495.

- [23] CHEN Xiao-guang, XIE Rui-shan, LAI Zhi-wei, LIU Lei, ZOU Gui-sheng, YAN Jiu-chun. Ultrasonic-assisted brazing of Al–Ti dissimilar alloy by a filler metal with a large semi-solid temperature range [J]. *Materials & Design*, 2016, 95: 296–305.
- [24] LAI Zhi-wei, XIE Rui-shan, PAN Chuan, CHEN Xiao-guang, LIU Lei, WANG Wen-xian, ZOU Gui-sheng. Ultrasound-assisted transient liquid phase bonding of magnesium alloy using brass interlayer in air [J]. *Journal of Materials Science & Technology*, 2017, 33: 567–572.
- [25] LI Ming-yu, LI Zhou-lin, XIAO Yong, WANG Chun-qing. Rapid formation of Cu/Cu₃Sn/Cu joints using ultrasonic bonding process at ambient temperature [J]. *Applied Physics Letters*, 2013, 102(9): 31.
- [26] LI Yi-nan, YANG Cheng-fei, PENG Zi-long, WU Zhi-yuan, CUI Zhuang. Microstructure and formation mechanism of ultrasound-assisted transient liquid phase bonded magnesium alloys with Ni interlayer [J]. *Materials*, 2019, 12(22): 3732.
- [27] LI Zheng-wei, XU Zhi-wu, ZHU Da-wei, MA Zhi-peng, YAN Jiu-chun. Control of Mg₂Sn formation through ultrasonic-assisted transient liquid phase bonding of Mg to Al [J]. *Journal of Materials Processing Technology*, 2018, 255: 524–529.
- [28] GU Xiao-yan, SUI Cheng-long, LIU Jing, LI Dong-lai, MENG Zheng-yu, ZHU Kai-xuan. Microstructure and mechanical properties of Mg/Al joints welded by ultrasonic spot welding with Zn interlayer [J]. *Materials & Design*, 2019, 181: 108103.
- [29] ZHANG Jian, LUO Guo-qiang, WANG Yi-yu, XIAO Yuan, SHEN Qiang, ZHANG Lian-meng. Effect of Al thin film and Ni foil interlayer on diffusion bonded Mg–Al dissimilar joints [J]. *Journal of Alloys and Compounds*, 2013, 556: 139–142.
- [30] PENG Zi-long, ZHOU Tao-shuai, LI Yi-nan, CUI Zhuang, WU Zhi-yuan, YAN Jiu-chun. Microstructure and mechanical performance of AZ31/2024 dissimilar alloy joints using a multi-interlayer of Ni/Al/Zn via ultrasonic-assisted transient liquid phase bonding [J]. *Materials & Design*, 2021, 197: 109218.
- [31] LI Yi-nan, CUI Zhuang, WU Zhi-yuan, YAN Jiu-chun, PENG Zi-long, ZHOU Tao-shuai. Influence of Ni/Al/Zn multi-interlayers on microstructure and mechanical performance of AZ31/2024 dissimilar alloy brazing joints [J]. *The Chinese Journal of Nonferrous Metals*, 2021, 31(6): 1526–1535. (in Chinese)
- [32] WANG Ting, ZHANG Bing-gang, CHEN Guo-qing, FENG Ji-cai, TANG Qi. Electron beam welding of Ti-15-3 titanium alloy to 304 stainless steel with copper interlayer sheet [J]. *Transactions of Nonferrous Metals Society of China*, 2010, 20(10): 1829–1834.
- [33] ZHANG Bing-gang, WANG Ting, DUAN Xiao-hui, CHEN Guo-qing, FENG Ji-cai. Temperature and stress fields in electron beam welded Ti-15-3 alloy to 304 stainless steel joint with copper interlayer sheet [J]. *Transactions of Nonferrous Metals Society of China*, 2012, 22(2): 398–403.
- [34] YUAN Xin-jian, SHENG Guang-min, LUO Jun, LI Jia. Microstructural characteristics of joint region during diffusion-brazing of magnesium alloy and stainless steel using pure copper interlayer [J]. *Transactions of Nonferrous Metals Society of China*, 2013, 23(3): 599–604.
- [35] VARMAZYAR J, KHODAEI M. Diffusion bonding of aluminum-magnesium using cold rolled copper interlayer [J]. *Journal of Alloys and Compounds*, 2019, 773: 838–843.
- [36] HUANG Zhe-yuan, DU Hui-qiao, LIU Lei, LAI Zhi-wei, CHEN Xiao-guang, LONG Wei-min, WANG Wen-xian, ZOU Gui-sheng. Ultrasonic effect mechanism on transient liquid phase bonding joints of SiC_p reinforced Mg metal matrix composites using Zn–Al–Zn multi-interlayer [J]. *Ultrasonics Sonochemistry*, 2018, 43: 101–109.
- [37] LAI Zhi-wei, CHEN Xiao-guang, PAN Chuan, XIE Rui-shan, LIU Lei, ZOU Gui-sheng. Joining Mg alloys with Zn interlayer by novel ultrasonic-assisted transient liquid phase bonding method in air [J]. *Materials Letters*, 2016, 166: 219–222.
- [38] YAO Zhe-he, KIM G Y, WANG Zhi-hua, FAIDLEY L, ZOU Qing-ze, MEI De-qing, CHEN Zi-chen. Acoustic softening and residual hardening in aluminum: Modeling and experiments [J]. *International Journal of Plasticity*, 2012, 39: 75–87.
- [39] SIDDIQ A, GHASSEMIEH E. Thermomechanical analyses of ultrasonic welding process using thermal and acoustic softening effects [J]. *Mechanics of Materials*, 2008, 40(12): 982–1000.
- [40] WU J S, KUO K H. Decagonal quasicrystal and related crystalline phases in Mn–Ga alloys with 52 to 63 a/o Ga [J]. *Metallurgical & Materials Transactions A*, 1997, 28(3): 729–742.
- [41] BOKHONOV B, KONSTANCHUK I, IVANOV E, BOLDYREV V. Stage formation of quasi-crystals during mechanical treatment of the cubic Frank–Kasper phase Mg₃₂(Zn,Al)₄₉ [J]. *Journal of Alloys and Compounds*, 1992, 187: 2099–2100.
- [42] TSAI A P, INOUE A, MASUMOTO T. Icosahedral, decagonal and amorphous phases in Al–Cu–M (M= Transition Metal) systems [J]. *Materials Transactions JIM*, 1989, 30(9): 666–676.
- [43] MIZUTANI U, TAKEUCHI T, SATO H. Interpretation of the Hume–Rothery rule in complex electron compounds: γ -phase Cu₅Zn₈ alloy, FK-type Al₃₀Mg₄₀Zn₃₀ and MI-type Al₆₈Cu₇Ru₁₇Si₈ 1/1–1/1–1/1 approximants [J]. *Progress in Materials Science*, 2004, 49(3/4): 227–261.
- [44] TAN Cai-wang, ZANG Cheng-wei, XIA Hong-bo, ZHAO Xiao-ye, ZHANG Kai-ping, MENG Sheng-hao, CHEN Bo, SONG Xiao-guo, LI Li-qun. Influence of Al additions in Zn-based filler metals on laser welding–brazing of Al/steel [J]. *Journal of Manufacturing Processes*, 2018, 34: 251–263.
- [45] LI Yu-long, LIU Yan-ru, YANG Jin. First principle calculations and mechanical properties of the intermetallic compounds in a laser welded steel/aluminum joint [J]. *Optics & Laser Technology*, 2020, 122: 105875.
- [46] DONG Y P, LI Y L, ZHOU S Y, ZHOU Y H, DARGUSCH M S, PENG H X, YAN M. Cost-affordable Ti–6Al–4V for additive manufacturing: Powder modification, compositional modulation and laser in-situ alloying [J]. *Additive*

- Manufacturing, 2021, 37: 101699.
- [47] QIAO Zhi-ya, YAN Li-jun, CAO Zhan-min, XIE Yu-nan. Surface tension prediction of high-temperature melts [J]. Journal of Alloys and Compounds, 2001, 325: 180–189.
- [48] SEMADENI F, BALUC N, BONNEVILLE J. Mechanical properties of Al–Li–Cu icosahedral quasicrystals [J]. Materials Science and Engineering A, 1997, 234/235/236: 291–294.
- [49] XU Zhi-wu, LI Zheng-wei, PENG Li-ming, YAN Jiu-chun. Ultra-rapid transient liquid phase bonding of Mg alloys within 1 s in air by ultrasonic assistance [J]. Materials & Design, 2019, 161: 72–79.

Mg–Al–Zn 三元金属间化合物对采用 Al/Zn/Cu/Zn 复合中间层的 MB8/2024 超声辅助钎焊接头的增强作用

李 婕¹, 石 磊², 李一楠¹, 周韬帅¹, 于子京¹, 张鸿昌¹, 彭子龙¹, 苗树文³, 高建国³, 苏昭方³

1. 青岛理工大学 机械与汽车工程学院, 青岛 266000;
2. 浙江亚通焊材有限公司, 杭州 310000;
3. 山东经典重工集团有限公司, 济宁 272100

摘 要: 研究采用 Al/Zn/Cu/Zn 复合中间层的 MB8/2024 超声辅助钎焊接头的显微组织演变规律。结果表明, 在 MB8 母材与铜箔之间添加铝箔可实现这两者界面上的金属间化合物由 Al_3Mg_2 向 $\text{AlMg}_4\text{Zn}_{11}$ 的转变。这个转变增强接头的力学性能, 并且在超声作用 22 s 时获得最高剪切强度为 85.26 MPa 的接头。热力学分析表明, Al_3Mg_2 和 $\text{AlMg}_4\text{Zn}_{11}$ 的吉布斯自由能分别为 -31.94 kJ/mol 和 -38.65 kJ/mol , 这为该转变提供热力学基础。由于空化效应的影响, 首次在超声辅助钎焊中发现 $\text{Mg}_{32}(\text{Al,Zn})_{49}$ 准晶。

关键词: Al/Zn/Cu/Zn 复合中间层; 超声辅助钎焊; 金属间化合物; 相转变; 力学性能; 准晶

(Edited by Bing YANG)